JOURNAL OF MATERIALS SCIENCE 18 (1983) 1267–1290

Review
An overview of ion sputtering physics and practical implications

JEAN-CLAUDE PIVIN
Laboratoire de Métallurgie Physique, Bât. 413,Université Paris-Sud, Centre d'Orsay, 91405 Orsay cedex, France

The first part of this review surveys the forms of energy exchange between incident ions and target atoms, going on to an examination of the distribution in depth of deposited energy. This analysis is then used to interpret the sputtering yield under various circumstances. The last part of the paper is devoted to a survey of different forms of radiation damage in sputtered targets, with special reference to the many factors that modify the original composition profile: such modification is related to the bombardment conditions used in analytical techniques such as AES, ESCA or SIMS which may be used, *inter alia*, to determine composition profiles.

1. Introduction

The bombardment of a solid by a beam of ions of selected mass and energy induces the formation of much residual damage in the target and the emission of various species such as backscattered ions, sputtered atoms and clusters, secondary and Auger electrons, light and X-rays (see Fig. 1), each providing a distinct mode of surface analysis [1]. This damage and these emissions result from the progressive slowing down of the incoming ion, via elastic scattering by the atom cores and via inelastic scattering by electron shells and free electrons. The ion is implanted at a depth depending on its energy and on the scattering sequence; a few are backscattered in vacuum. Targets atoms are displaced from their equilibrium sites during elastic collisions with the incident ion. These recoiling atoms displace other target atoms in their turn, and a complex collision cascade is set up. A large number of atoms are set in motion during this cascade of primary and secondary recoils (Fig. 1).

A small fraction of the atoms set in motion are sputtered. Most come to rest on other sites and contribute to a mixing of atomic layers. Other forms of radiation damage are the implantation of ions, selective displacements of species during the collision cascade according to their masses and binding energies, and enhanced diffusion due to residual defects. All these forms of damage contribute to change the composition and structure of the target.

Sputtered atoms were well defined by Sigmund [2] as one particular variant of the various types of radiation damage created during the collision cascade. Sputtered atoms may be characterized as the flux of atoms moving toward the target surface, with an energy large enough not to be scattered in other directions and to overcome the surface potential. Only atoms issuing from the outermost layers have a noticeable probability of fulfilling these conditions. Thus the number of sputtered atoms N_s per incident ion is closely related to the number of atoms set in motion N_d and their depth distribution. The number of displaced atoms depends on the energy E_1 of the incoming ions and on the displacement energy E_d, which is entirely characteristic of the target structure and composition. Their distribution depends on the displacement cross-section σ_d of target atoms by ions and secondary projectiles set in motion at various depth with an energy greater than E_d. It is closely connected with the law of slowing down of incident ions and their mean penetration depth.

0022–2461/83 $03.00 + .12

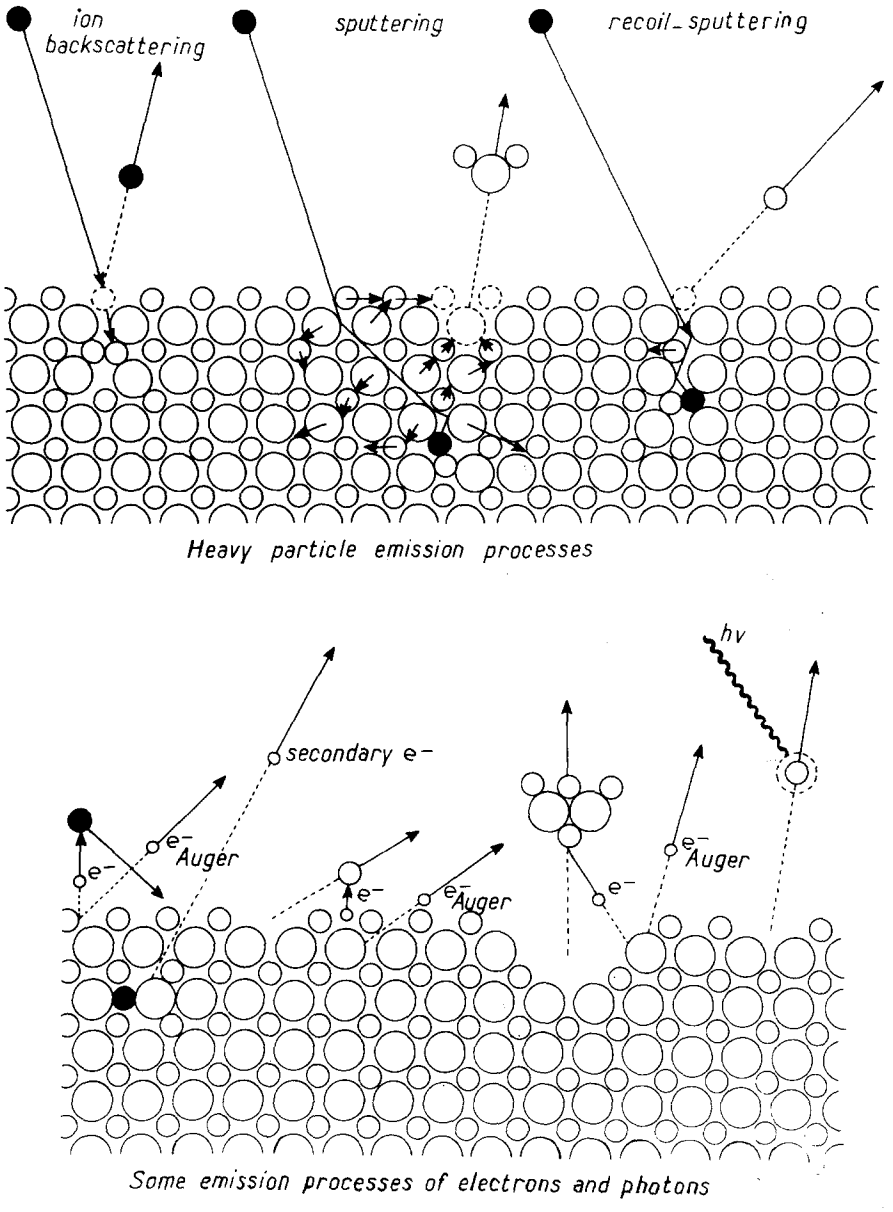

Figure 1 Emission processes induced by the bombardment of a target by an ion beam.

Thus the first section of this paper will be devoted to giving a feel for the energy exchanges which occur between projectiles of various energy (incident ions and recoiling atoms) and atoms at rest in the lattice. The conclusion of this section will be the formulation of energy losses as a function of E_1 and of the atomic parameters of incident ions and target atoms, according to the theory of Lindhard, Scharff and Schiøtt [1, 3–6]. The account which will be presented in Sections 2 and 3, of the depth distribution of the deposited energy and of the correlation between this distribution and the sputtering yield S (equal to N_s), is greatly indebted to Sigmund's papers on the topic [2, 7–10]. The second part of this paper is devoted to a discussion of the balance between sputtering and other forms of radiation damage, with particular reference to the bombardment conditions used in Auger electron spectroscopy, electron spectroscopy for chemical analysis or secondary ion mass spectrometry (AES, ESCA, or SIMS).

Our purpose is not to review up-to-date calculations of the amount of the various types of radiation damage, but to provide the necessary scientific basis for investigators concerned with the analysis of the surfaces of materials.

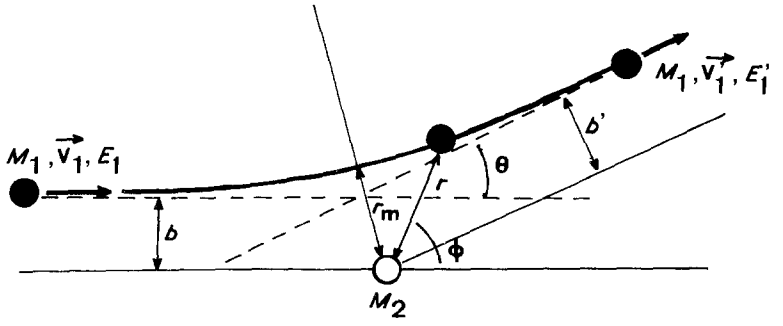

Figure 2 Scattering of a particle (M_1, v_1, E_1) by an atom (M_2) at rest: – trajectory ------ asymptotes. The energy transfered to atom 2 is $T = E_1 - E_1'$.

2. Energy losses

In the theory of Lindhard, Scharff and Schiøtt (LSS theory) [3], the elastic energy losses, due to a scattering of the incident particle (M_1, $\mathbf{v}_1$, E_1) in the electric field of atoms, and the inelastic losses are considered separately. Let x denote the depth below the surface and dE_1/dx the differential energy loss or stopping power of an infinitesimal thickness dx of the target. It is equal to the sum of a nuclear stopping power, $(dE_1/dx)_n$, and an electric one, $(dE_1/dx)_e$: then

$$\left(\frac{dE_1}{dx}\right) = \left(\frac{dE_1}{dx}\right)_n + \left(\frac{dE_1}{dx}\right)_e$$

$$= N[\sigma_n(E_1) + \sigma_e(E_1)]$$

in which N is the number of scattering centres or atoms in the thickness dx, and $\sigma_n(E_1)$, $\sigma_e(E_1)$ the nuclear and electronic stopping cross-sections of each scattering centre.

2.1. General considerations on the elastic scattering of a particle in the electric field of an atom at rest

The reader should refer to references [11] and [12] for background material on the treatment of elastic and inelastic scattering. Important parameters of the elastic scattering of a particle (M_1, $\mathbf{v}_1$, e_1) by a motionless atom M_2 are indicated in Fig. 2. Let (i) r and ϕ denote the coordinates of the trajectory of the incident particle 1 in a relative frame of reference with origin at atom 2, (ii) b the impact parameter (b is the distance between the tangent to the trajectory of the incoming ion and a parallel line passing through M_2, which would correspond to a head-on collision with the same speed $\mathbf{v}_1$), (iii) E_r the relative energy of particle 1, and (iv) $V(r)$ its potential energy.

One can obtain a simple relation between these parameters by writting the laws of the conservation of the energy and momentum:

$$\frac{b^2}{r_m^2} = 1 - \frac{V(r_m)}{E_r} \tag{1}$$

with

$$E_r = E_1 \frac{M_2}{M_1 + M_2} \tag{2}$$

This equation accounts for the observation that, for a given impact parameter b, the distance of closest approach r_m decreases with increasing relative energy. Meantime, the potential energy $V(r_m)$ becomes more repulsive. When considering the classical scheme of the potential energy as a function of the distance between atoms r, the potential is attractive for values of r greater than the equilibrium distance D in the chemical bond 1–2, and it is repulsive for values of r lower than D. Nuclear scattering occurs only in this last case. Thus the scattering angle θ of the incoming particle and the kinetic energy T transferred to atom 2 depends on b and E_1: they increase when E_1 and b decrease. A differential scattering cross-section must be defined for each pair of values b, E_1. This differential cross-section $d\sigma(E_1, b)$ corresponds to to one scattering event with a potential $V(r_m)$, a transferred energy T and a scattering angle θ. It is generally expressed as a function of two other variables related to b and E_1: $d\sigma(E_1, T)$ or $d\sigma(E_1, \theta)$.

2.2. Choice of an analytical form of the potential $V(r)$

An important hypothesis for further calculations is that $V(r)$ is a steady-state function, i.e. independent of the electronic exchange energy (which increase when r decreases).

The most straightforward expression for the repulsive potential between nuclei is the Coulomb potential $V(r) = Z_1 Z_2 e^2/r$. But the value of this potential is too high for distance r greater than $0.5D$. For values of r ranging from 0.5 to $1D$ the screening effect of the nuclear charge by its

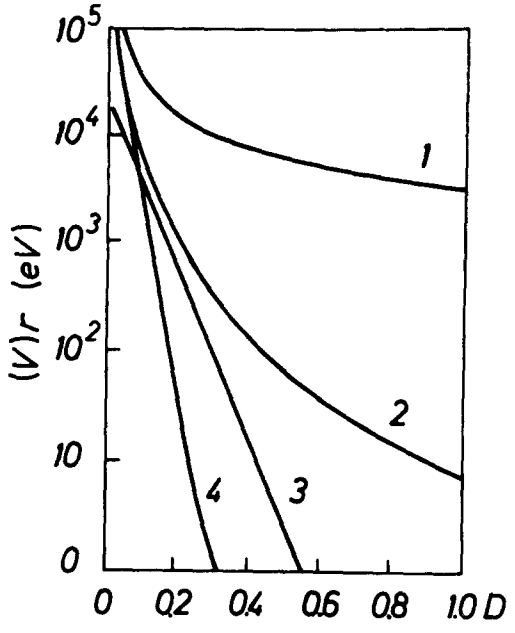

Figure 3 Interatomic potentials for copper [12]: (1) Coulomb potential, (2) Thomas–Fermi potential, (3) Born–Mayer potential, (4) Bohr potential. D is the lattice constant (0.255 nm).

electron core must be taken into account. The Coulomb potential is balanced by a screening function $\psi(r/a)$, as follows:

$$v(r) = \frac{Z_1 Z_2 e^2}{r} \psi(r/a) \qquad (3)$$

in which a is a screening radius.

Various functions $V(r)$ have been proposed, whose validity depends on the value of r. The most useful are the Bohr potential (valid for $r \ll 0.1$ nm), the Thomas–Fermi potential, and the purely exponential potential $Ae^{-r/a}$ proposed by Born–Mayer (valid for $r \gg 0.1$ nm). They are summarized on Fig. 3 [12].

Lindhard proposed a common approximation to all these potentials, of the form:

$$V(r) = Z_1 Z_2 e^2 \frac{a^{n-1}}{nr^n} \qquad (4)$$

in which n varies according to the distance of closest approach r_m or to the energy E_1 of the incident particle.

The value $n = 1$ corresponds to a Coulomb potential, describing a Rutherford-type scattering; $n = 2$ or 3 correspond to a Thomas–Fermi potential and values of $n \gg 1$ to a Born–Mayer one. The limiting value $n = \infty$ describes the collision of a point particle M_1 with a hard sphere. Schematically, the incident atom 1 sees the atom at rest 2 as a billiard ball or penetrates a deadening gas of electrons.

2.3. Values of the elastic stopping power

The analytical forms of $d\sigma(E_1, T)$ corresponding to the above-mentioned potentials are summarized in Table I. They are expressed as a function of the parameter $m = 1/n$ involved in Equation 4.

The stopping cross-section of particles incoming with an energy E_1 and with various b – and scattered in various directions with different values of T – is the mean scattering cross-section over all values of b, θ or T:

$$\sigma_n(E_1) = \int_b d\sigma_n(E_1, b) = \int_T d\sigma_n(E_1, T) = \int_\theta d\sigma_n(E_1, \theta) \qquad (5)$$

Note that the displacement cross-section σ_d is the partial integration over kinetic energies T transferred to the nucleus, ranging from the displacement energy E_d to E_1.

2.4. Values of the inelastic stopping power

Let Q be the energy transferred to electron shells by the incident particle during inelastic collisions. Fig. 4 shows the variation of Q with the distance of closest approach r_m [11]. $Q(r_m)$ values may be deduced from spectroscopic data on the cross-

TABLE I

E_1/M_1	$V(r)$	m	σ_e	$d\sigma_n = C_m E_1^{-m} \frac{dT}{T^{1+m}}$
> 100 keV(amu)$^{-1}$	Coulomb	1	k/E_1	$\frac{C_m dT}{E_1 T^2}$
> 10 eV(amu)$^{-1}$	Thomas–Fermi	1/2 or 1/3	$kE_1^{1/2}$	$\frac{C_m dT}{E_1^{1/2} T^{3/2}}$
< 10 eV(amu)$^{-1}$	Born–Mayer	0	very low	$\frac{C_0 dT}{T}$

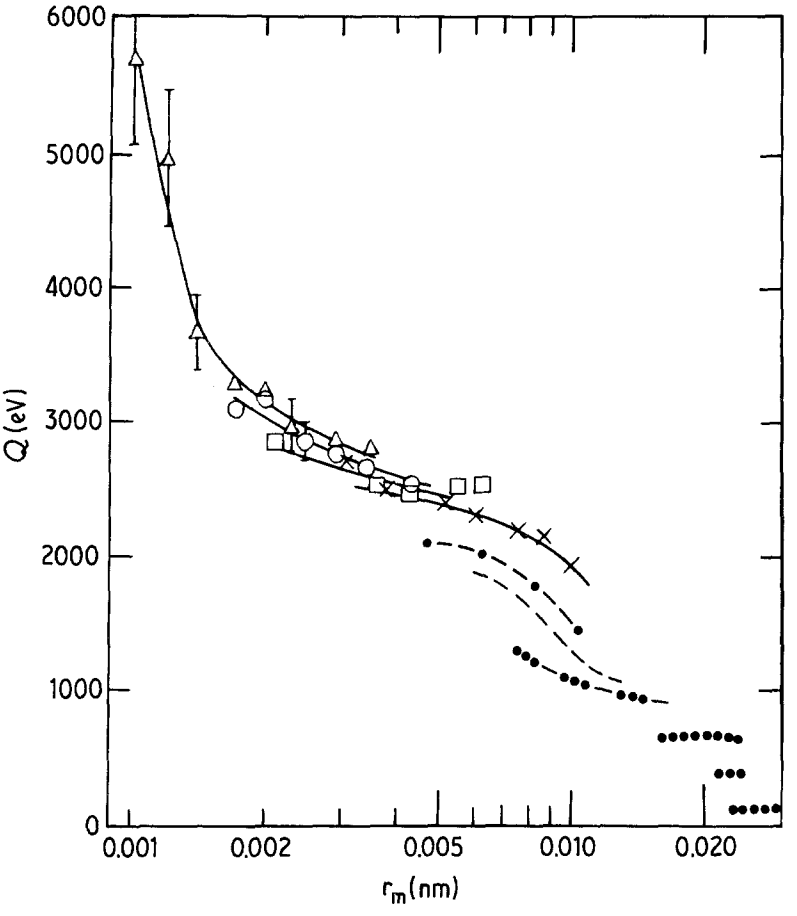

Figure 4 Average inelastic energy loss Q as a function of the distance of closest approach r_m, for various projectile energies [11]. These experimental results were obtained by Kessel *et al.* (1969) for Ar^+–Ar collisions.

sections of various transitions between energy levels of electrons and the cross-section of ionization of atoms.

Note that r_m values lower than 0.010 nm correspond to high energy ions (E_1/M_1) of the order of 1 MeV (atomic mass unity)$^{-1}$. For medium and low energies, individual inelastic energy losses $Q(r_m)$ remain negligible when compared to E_1. In these conditions, inelastic energy losses will be treated as due to a friction force exercised by an electron gas on the incoming particle, rather than to individual scatterings with various transferred energies Q and angles θ.

This friction force results in:

1. An ionization of the electron gas by high-energy particles $(E_1/M_1 > 100\,\text{keV(amu)}^{-1})$. This interaction is described by an energy dependence of the $\sigma_e(E_1) = k/E_1$, where k is a constant that depends on Z_1, Z_2, M_1, M_2;

2. Excitation and ionization processes for medium energy particles $(E_1/M_1 > 10\,\text{eV(amu)}^{-1})$, which correspond to the energy range of ions used for sputtering experiments. Using a Thomas–Fermi model, Lindhard calculated $\sigma_e(E_1) = kE_1^{1/2}$;

3. Individual excitations of electrons in valence bands or of electrons of conduction, and collective longitudinal excitation of the conduction electron gas (plasmons), for particles with an energy lower than 10 eV(amu)$^{-1}$. In this case, a simple law of the type $\sigma_e(E_1) = f(E_1)$ has not as yet been determined.

2.5. The balance between nuclear and electronic stopping powers in the medium energy range

Fig. 5 shows the variations of both nuclear and electronic stopping powers as a function of the energy in a dimensionless universal system $d\epsilon/d\rho = f(\epsilon)$; the reduced energy ϵ and depth ρ are independent of the mass and the atomic number of ions and target atoms [12].

The nuclear stopping power is greater than the electronic one in the case of ions of relatively low energy and medium mass. For instance, the stopping powers of 1 keV argon ions by a silicon or nickel target are comparable and equal to

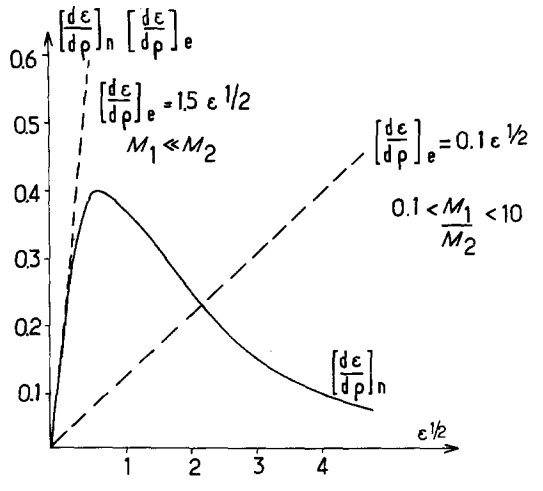

Figure 5 Nuclear and electronic stopping powers in reduced units: $\epsilon = E_1[M_2/(M_1+M_2)]\{a_0/[e^2 Z_1 Z_2 (Z_1^{2/3}+Z_2^{2/3})^{1/2}]\}$; $\rho = x 4\pi N[a_0^2/(Z_1^{2/3}+Z_2^{2/3})][M_1 M_2/(M_1+M_2)]$; a_0 being the Bohr radius of the hydrogen atom. $k = 1.5$ for protons and $k = 0.1$ for argon ions in most materials.

$(d\epsilon/d\rho)_n = 0.4$ and $(d\epsilon/d\rho)_e = 0.03$, i.e. $(dE_1/dx)_n$ of the order of 10^{-2} keV nm^{-1} and $(dE_1/dx)_e$ of the order of 10^{-3} keV nm^{-1}. This accounts for the usual choice of argon ions with an energy in the range 0.5 to 5 keV in sputtering experiments. In these experimental conditions the greater part of the energy of the incoming ions is transferred to atoms.

2.6. Correlation between the sputtering yield $S(E_1)$ and $(dE_1/dx)_n$

This correlation is clear since the number of displaced atoms must depend on the stopping power of nucleus. It is illustrated in Fig. 6, for the case of a copper target bombarded with Kr^+ ions [2]. The sputtering yields were obtained by measuring weight losses of a polycrystalline copper target, and the energy losses $(dE_1/dx)_n$ were calculated by means of the LSS theory, summarized in previous Sections. The proportionality of $S(E_1)$ to

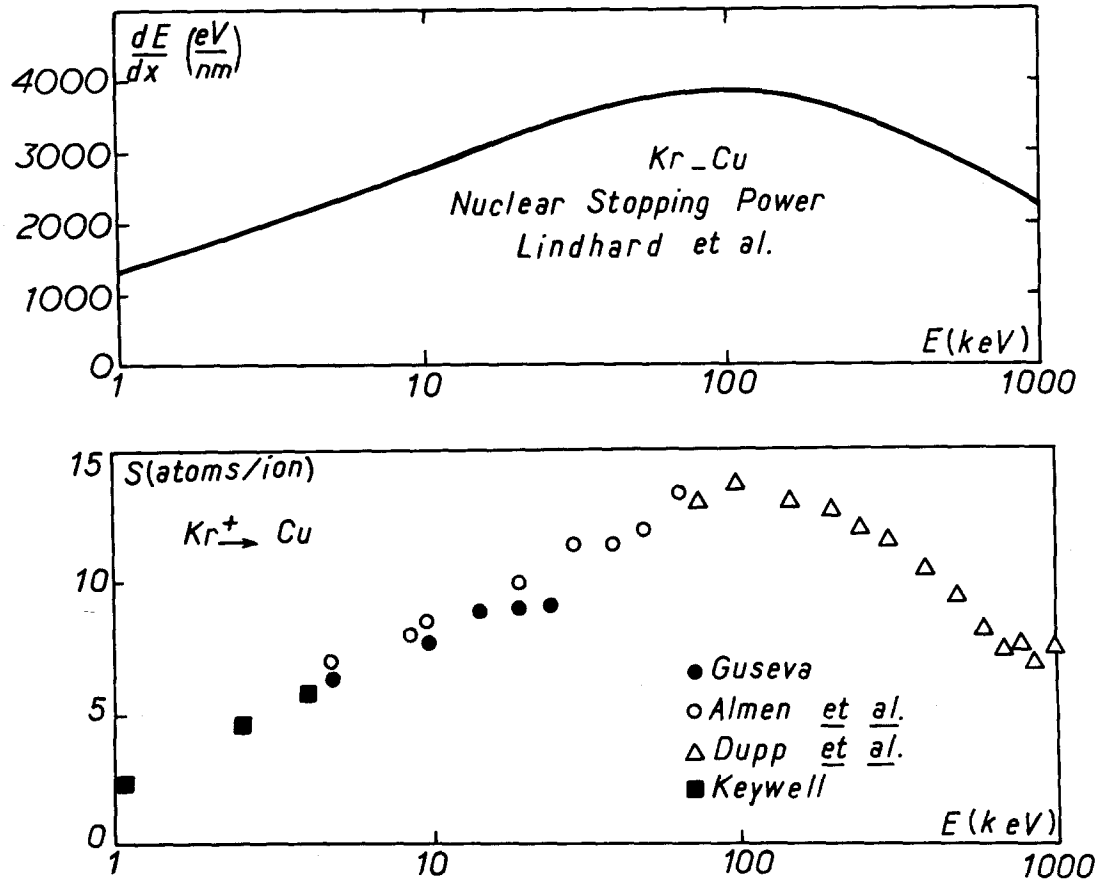

Figure 6 Measured sputtering yields for krypton ions on polycrystalline copper at normal incidence, and calculated nuclear stopping power [2].

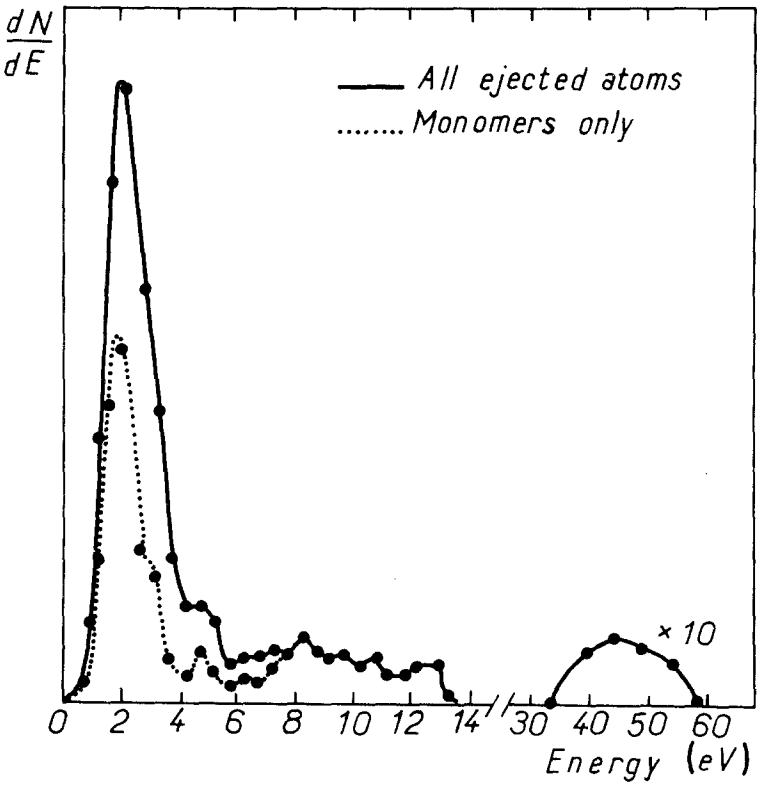

Figure 7 Energy distribution of atoms and clusters ejected from a copper target by 0.6 keV argon ions [16].

$(dE_1/dx)_n$ is general, whatever may be the target, for incoming ions of medium energy [13]:

$$S(E_1) \propto \left(\frac{dE_1}{dx}\right)_n \tag{6}$$

3. Depth distribution of the deposited energy and correlation with the sputtering yield

Generally, sputtering and the formation of point defects result from the dissipation of the energy of incoming ions during a linear cascade of binary collisions (primary collisions between the incoming ion and atoms at rest (I), secondary collisions between projectiles (I) set in motion and other atoms at rest (II), etc.). But, in some cases, the observed phenomena account for a more general agitation of atoms within a volume whose dimensions are of the order of the ion range. Such an agitation of atoms is called a spike [14]. The depth distribution of the deposited energy and the parameters of the sputtering yield are different in the two cases [2, 15].

3.1. Energy transfers during a linear collision cascade; energetic distribution of recoiling atoms and sputtered atoms

The energy deposited at each depth is transported mainly by incoming ions and atoms (I) displaced during primary collisions with the incident ions.

These primary recoiling atoms may be sputtered by a simple rebound or multiple rebound process [15]. These carry most part of the energy of sputtered particles. Those primary recoiling atoms which are not directly sputtered induce secondary, ternary collisions. A larger number of atoms are displaced during these collisions, but the kinetic energy of the projectiles decreases with the order of the collision. Consequently projectiles of second or third order can be sputtered only if located in the outermost layers of the surface before the collision cascade. This accounts for the dependence of S on the depth distribution of the deposited energy: the larger the fraction of the projectile energy deposited in the outermost layers, the higher the sputtering yield and the lower and the number of defects which are created in the bulk.

Sputtering of atoms by a cascade of secondary and tertiary collisions is designated a "slow collisional process", in opposition to the "quick collisional process" of rebound [15]. The difference in the kinetic energies of atoms sputtered by the two processes is illustrated in Fig. 7, which shows the energy distribution of atoms and

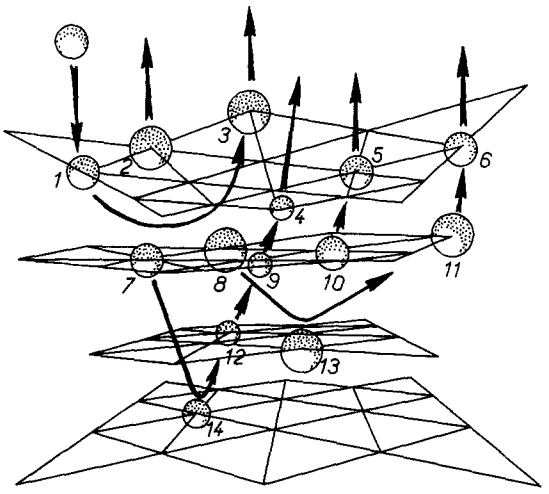

Figure 8 Simulated bombardment of a copper target with 0.6 keV argon ions. Only the atoms involved in the collision cascade are drawn. Other atoms are located at the intersections of the grid lines [16].

clusters ejected from a copper target by 0.6 keV argon ions. This distribution was deduced from computed simulations of collision cascades [16]. The small 50 eV peak corresponds to primary atoms sputtered by rebound; but most of the sputtered atoms, those ejected after two or more collisions, have kinetic energy in the range 1 to 4 eV.

Fig. 8 shows the computed simulation of one collision cascade [17]: sputtered atoms 2, 3, 4, 5, 6 issue from the outermost layer of the target and have a low kinetic energy. One must also note on this figure the evidence of a focused collision sequence (atoms 14, 12, 9, 4). These "focusons" occur essentially along atomic rows of high density; statistically they contribute only a few per cent to sputtering yields [22, 23].

3.2. Depth distribution of the energy deposited during a linear collision cascade; correlation with the sputtering yield

The depth distribution $f_1(x)$ of the energy deposited by incoming ions may be easily deduced from the energy losses [12]:

$$\left(\frac{dE_1}{dx}\right) = N[\sigma_n(E_1) + \sigma_e(E_1)] \qquad (7)$$

Consider an amorphous or polycrystalline target in order to eliminate the influence of the crystallographic orientation of the surface on the mean free path of incoming ions (channelling of ions entering the target along a direction parallel to dense atomic rows or planes). Consider also the case of ions of medium energies which are generally used for sputtering experiments. In this case, the distribution $f_1(x)$ of the deposited energy can be approximated by a Gaussian, because the energy of ions is essentially dissipated during elastic collisions. $f_1(x)$ represents also the distribution of ions which come to rest, i.e. implanted ions.

$$f_1(x) = \frac{1}{2\pi\langle\Delta x_1^2\rangle^{1/2}} \exp -\frac{|x-\langle x_1\rangle|^2}{2\langle\Delta x_1^2\rangle}$$

with

$$\langle\Delta x_1^2\rangle = (x-\langle x_1\rangle)^2 \qquad (8)$$

The mean implantation depth x_1 is given by the Lindhard equation:

$$\langle x_1\rangle = \frac{1}{N}\int_0^{E_1} \frac{dE}{\sigma_n(E)+\sigma_e(E)} \qquad (9)$$

The depth distribution $f(x)$ of the energy deposited by all the projectiles, during a cascade of elastic collisions, is also sensibly Gaussian. It also represents the depth distribution of atoms displaced during collisions of successive orders, i.e., the distribution of induced defects. The values of $\langle x\rangle$ and $\langle\Delta x^2\rangle$ are generally different for the two distribution $f_1(x)$ and $f(x)$ (see Fig. 9a), because the mean free path of primary recoiling atoms may not be neglected as compared to $\langle x_1\rangle$.

But functions of greater interest for the calculation of the sputtering yield are the integrations $F_1(x)$ and $F(x)$ of the energy deposited during elastic collisions on layers of thickness $(0, x)$. These functions are indicated in Fig. 9b. In this figure, $\nu(E_1)$ is the part of the energy E_1 transferred to recoiling atoms during the whole cascade. The energy taken out the target $F(x=0)$ is mostly transported by sputtered atoms, to a small extent by backscattered ions.

The sputtering yield is proportional to the part of the available energy which is deposited in the outermost layers of the target $F(x\simeq 0)$. On the other hand, the mean value of $F_1(x\simeq 0)$ is the stopping power of the target $(dE_1/dx)_n$ for ions entering an amorphous or polycrystalline surface with an energy E_1.

$F(x\simeq 0)$ differs from $F_1(x\simeq 0)$ by a factor α. α represents the proportion of displaced atoms in the outermost layers of the target. It represents the influences of various parameters such as: (i) the relative masses of incident ions and target atoms on the scattering angle of ions; (ii) the

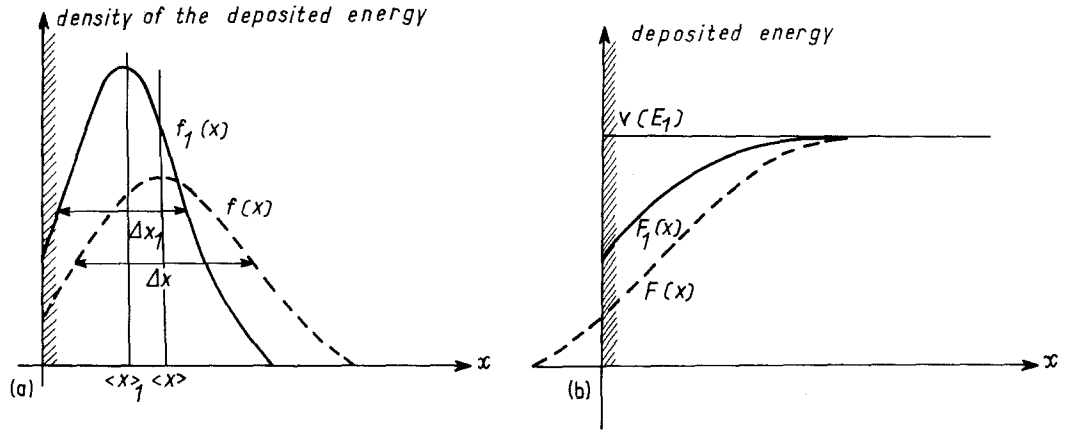

Figure 9 Schematic distribution of the deposited energy.

incidence angle of ions; (iii) the crystallinity of the target.

The last factor, Λ, of the sputtering yield, represents the probability that atoms displaced in the outermost layers will leave the target. A part of the incident energy $F(x \simeq 0)$ is deposited in the form of low kinetic energies transferred to secondary recoiling atoms. Only a fraction of these atoms move toward the surface. They may be stopped before emerging from the surface and they must overcome the surface potential barrier.

The analytical expression of the sputtering yield, then is:

$$S(E_1) = \Lambda F(x \simeq 0) = \Lambda\alpha\left(\frac{dE_1}{dx}\right)_n \quad (10)$$

Two procedures may be used to estimate the fraction of the energy deposited at each depth $f(x)$, and especially $F(x \simeq 0)$, S.

(a) The first one is based on the estimation of mean values of the stopping cross-section $\sigma_n(E)$ and of the displacement cross-sections $\sigma_d(E)$, or the mean free path of the various projectiles, by means of above Equations 7 to 10 and Table I [7, 18–20]. In the case of an amorphous target, the Boltzmann transport equation may be used to describe the different flux of particles in the target with various masses and speed at each instant t and at each depth x: $g(x, \mathbf{v}, M, t)$. Such a model was used by Sigmund to estimate S in monatomic targets [7], then in composite targets [20, 21], for low fluences of incoming ions (before any change in the superficial composition).

(b) Collision cascades may also be simulated by means of a computer, taking into account energy transfers during each collision (with various parameters E, b, T, θ). Such simulations were performed by several authors [16, 17, 22–25] using a Monte Carlo procedure. These calculations provide an estimation of the global sputtering yield but also energy and angular distributions of ejected particles, sputtering yields of clusters and an approach to their mechanism of formation [22, 25]. Moreover the dependence of the sputtering yield upon the crystallographic orientation of the surface with respect to the direction of incidence of the ion beam, may be taken into account [22, 23]. The variation of the sputtering yield of each element in a composite target with the fluence of ions (due to changes in the superficial composition) may be calculated [26], more easily than with a global estimation of the flux $gi(x, \mathbf{v}, Mi, t)$ of atoms i provided by various models [19, 20, 27–29].

However, the models proposed by Sigmund and other authors [7, 18, 19, 30] give analytical expressions of S as a function of the different macroscopic parameters: energy and incidence angle of ions, respective masses of ions and target atoms, surface potential, etc. They permit materials scientists using surface analytical techniques to estimate easily the variation of S with the conditions of bombardment and with the nature and composition of the target.

3.3. Depth distribution of the energy deposited during a spike

We defined spikes as a general agitation of atoms within the cascade volume, which can no more be described by binary collisions. Experimental evidence for the existence of spikes consists of measured values of the sputtering yield exceeding the result predicted from linear collision cascade theory, different energy distributions of the

sputtered particles and particular residual defects [2, 15, 31–41]. One must consider different concepts under the term "spike".

Collisional spikes occur for example in heavy targets bombarded with heavy ions, e.g. Xe^+, Kr^+, Au^+ ions bombarding a gold target [31, 32]. The difference between a linear collision cascade and a collisional spike is a matter of the number of atoms in motion in the cascade volume λ [14]. A discrete cascade occurs when there is a long mean free path between significant elastic collisions. On the contrary, the energy transferred to atoms $\nu(E_1)$ is deposited within a small volume in the case of a collisional spike. Let N be the number of atoms per unit volume. Almost all $(N\lambda)$ atoms are set in motion within the cascade volume λ when the mean energy transferred to each atom θ exceeds a critical value θ_0: [2]

$$\theta = \frac{\nu(E_1)}{N\lambda} > \theta_0 \qquad (11)$$

This critical value of the deposited energy density is much lower than the displacement energy of atoms during an individual elastic collision. Ruault *et al.* [32] observed residual defects in gold, which were characteristic of a spike, for values of $\theta \geqslant 2$ eV per atom. The spike may be assimilated to a local thermal agitation of atoms in a volume λ and θ to the "temperature of atoms", which is dissipated during a characteristic time τ for the decay of the temperature in the hot spot ($\tau \simeq 10^{-13}$ sec).

Other types of spikes occur in some insulators and ionic crystals (for example alkali halides) [35, 38, 40, 41], which were ascribed to particular dissipation mechanism of inelastic energy losses. However, while attempts have been made to develop a crude procedure for the estimation of $F(x)$ in a spike and of the sputtering yield S [2, 15, 20, 42], no calculations fitting experimental measurements of S have been made until today.

4. Estimation of the sputtering yield S within the linear cascade regime

4.1. Sigmund equation for an individual sputtering event on a monatomic and amorphous target

In such a case the Boltzmann equation describes the different flux of particles at each depth x in the target. Among particles moving in a layer $(x, x + dx)$, one must distinguish:

(a) incoming ions and primary recoiling atoms which have a Thomas–Fermi scattering cross-section,

(b) atoms of low kinetic energy, displaced during secondary recoils, which have a Born–Mayer scattering cross-section.

Variation in the amount $g(x, M, \mathbf{v}, t)$ of particles of a given mass and speed in each layer are due to the motion of atoms in and out the layer of thickness dx and to scattering events, during which new atoms are set in motion and the speed of incident particles is changed

$$\left(\frac{\partial g}{\partial t}\right)_{M,\mathbf{v},x} = \left(\frac{\partial g}{\partial t}\right)_{M,\mathbf{v},x}^{\text{collisions}} + v_x \cdot \text{grad}_x(g) \qquad (12)$$

A definitive value must be ascribed to the displacement energy E_d to determine the amount of atoms set in motion during collisions. In an amorphous target E_d is isotropic; its value is the cohesive energy per atom in the sputtered phase.

The whole development of the calculations will not be presented here; we will follow a simplified approach as presented by Sigmund in one of his more recent papers [2].

4.1.1. Estimation of the number of displaced atoms in outermost layers

Values of the energy deposited at each depth and of the factor α are deduced from estimates of the flux of ions and primary recoiling atoms at each depth during the whole collision cascade. The transport theory predicts a $(\cos\theta)^{-f}$ dependence of α on the incidence angle θ of ions with respect to the normal to the surface. f is a function of masses M_1, M_2 and of the exponent m involved in the analytical formula of the scattering cross-section. In the case of argon ions of a few keV and for not too heavy target atoms ($M_2 < 100$), f is about equal to 5/3. Fig. 10 shows a comparison of the calculated evolution of the sputtering yield as a function of θ with experimental value of $S(\theta)$ [7]. For angles greater than 70° the measured sputtering yield decreases, because most part of the incident ions are backscattered by atoms of the outermost layer.

The value of α for a normal incidence, α_N, depends also on respective masses M_1, M_2 and on the exponent m of the interaction law. Fig. 11 shows a comparison of the calculated and measured variations [2, 9, 43]. In the case of target atoms not too heavy with respect to the mass of ions, the value of $\alpha_N(M_2/M_1)$ is about 0.2.

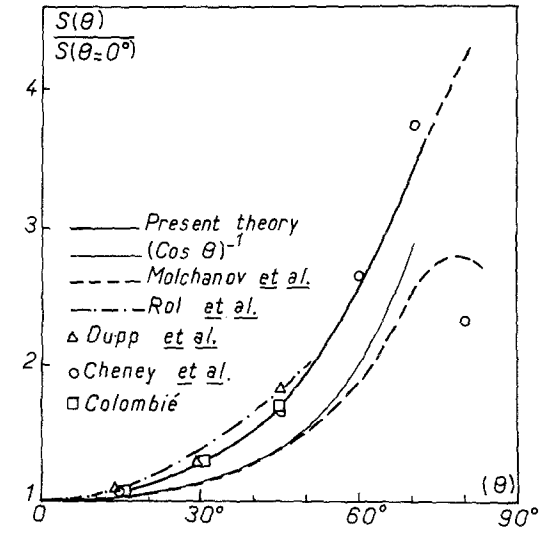

Figure 10 Variation of the sputtering yield with angle of incidence for argon ions bombarding a polycrystalline copper target [7]. The thick solid curve correspond to the $\cos\theta^{-5/3}$ dependence predicted by Sigmund calculations. A $\cos\theta^{-1}$ dependence would reflect the ratio of velocities v_{1x}/v_1. Other curves and points are experimental data.

4.1.2. Estimation of their ejection probability

The sputtering yield is the integration over the whole duration of the cascade of the flux of target atoms $g(x = 0, M_2, \mathbf{v}, t)$ moving outward the surface plane $x = 0$ with a component of speed v_x in direction x large enough to overcome the surface potential barrier, U_s:

$$v_x > \left(\frac{2U_s}{M_2}\right)^{1/2} \tag{13}$$

U_s is considered as a constant equal to half the value of E_d. In metallic targets U_s may be approximated by the sublimation energy. The factor Λ accounts for the angular distribution of their speeds (v_x must be negative) their stopping cross-section and the surface potential. It is equal to:

$$\Lambda = \frac{3}{4\pi^2}\frac{1}{C_0 U_s} = \frac{0.0420}{U_s} \tag{14}$$

where C_0 is the screening factor of the Born–Mayer cross-section (see Table I).

The resulting value of the sputtering yield is:

$$S = \frac{3}{4\pi^2}\frac{1}{C_0 U_s}\alpha_N(M_2/M_1)\cos\theta^{-5/3}\frac{1}{N}\left(\frac{dE_1}{d_x}\right)_n \tag{15}$$

4.2. Comparison with experimental results

The Sigmund model provides calculated values of S fitting well the measured values in most monatomic materials. It was shown in previous Sections that experience conforms the predicted correlation between S and the nuclear stopping power (Fig. 6) and the incidence angle of ions (Fig. 10).

S varies with the energy of incident ions as $(dE_1/dx)_n$ (Fig. 12). It depends on the mass of incident ions (Fig. 12) by means of stopping power $(dE_1/dx)_n$ and α_N. The calculated value increases continuously with M_1. The experimental evolution obtained by Almen and Bruce [13] is shown on Fig. 13: a large number of ions and three different targets of increasing masses are considered. Lastly, S presents the same periodicity

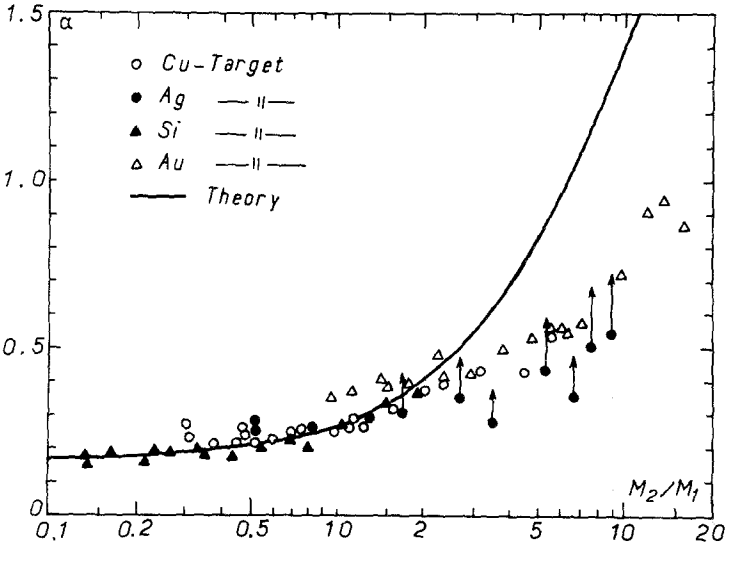

Figure 11 Variation of α at normal incidence with the ratio of masses M_2/M_1 [9, 37, 43]. The factor α was deduced from measured yields S of silicon, copper, silver, gold targets bombarded with various 45 keV ions. Corrections for electronic stopping and surface effect improve the agreement at large mass ratios.

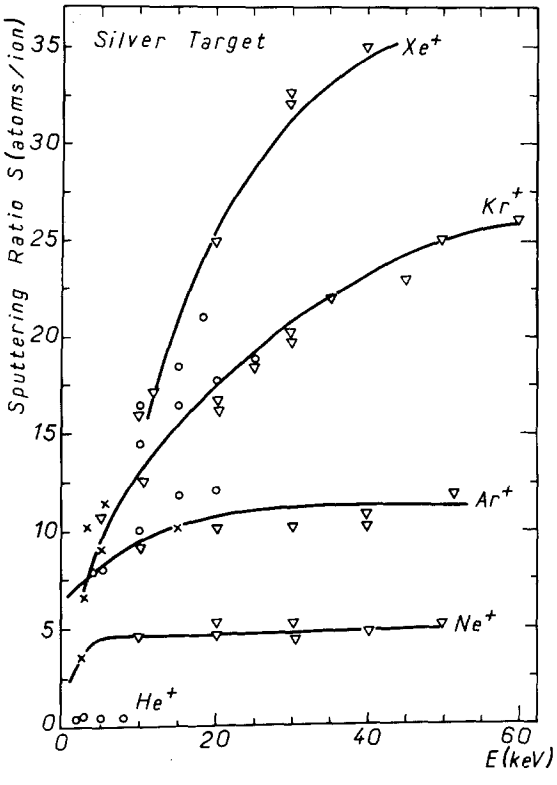

Figure 12 Variation of the sputtering yield with the mass and energy of ions, for a silver target bombarded with various noble gas ions [44].

as a function of the atomic number of target atoms as does the surface binding energy (Fig. 14) [13, 44].

The usual values of S in polycrystalline targets bombarded by argon ions of a few keV are in the range 1 to 10 atoms/incident ion. The depth x_0 from which most sputtered atoms issue is independent of the energy of incoming ions. Sigmund calculated that x_0 is of the order of 2 atomic rows, i.e. 0.5 nm for a copper target [7].

4.3. Interpolation of this model for individual sputtering events in polyatomic targets [20, 30]

The partial sputtering yield S_i' of the i component in the polyatomic target (noted ') may be written:

$$S_i'(E_1) = C_i \Lambda_i F'(x \simeq 0) \qquad (16)$$

in which C_i is the atomic concentration of the i component, Λ_i' the probability for i atoms displaced in outermost layers to leave the surface, and $F'(x \simeq 0)$ the part of the energy deposited near the surface in the polyatomic target.

For a target composed of elements of almost equal masses, the parameters of the cascade have nearly the same values in the elemental i target and in the polyatomic one. Thus the sputtering

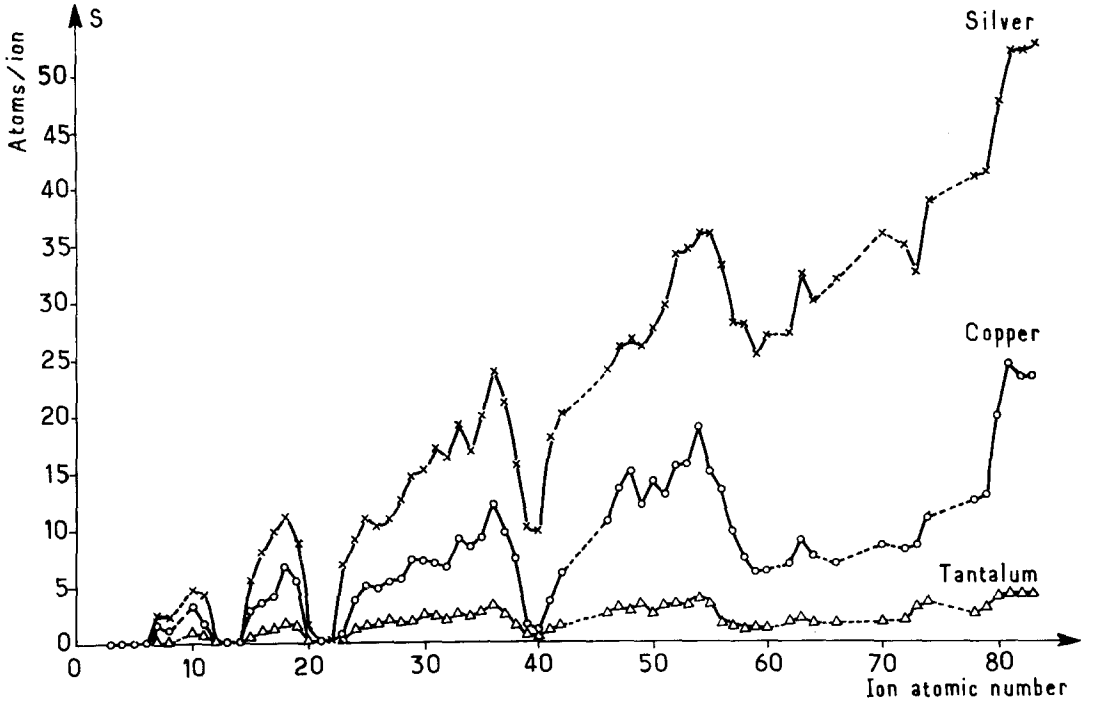

Figure 13 Variation of the sputtering yield with the atomic number of target atoms for 400 eV argon ions [44].

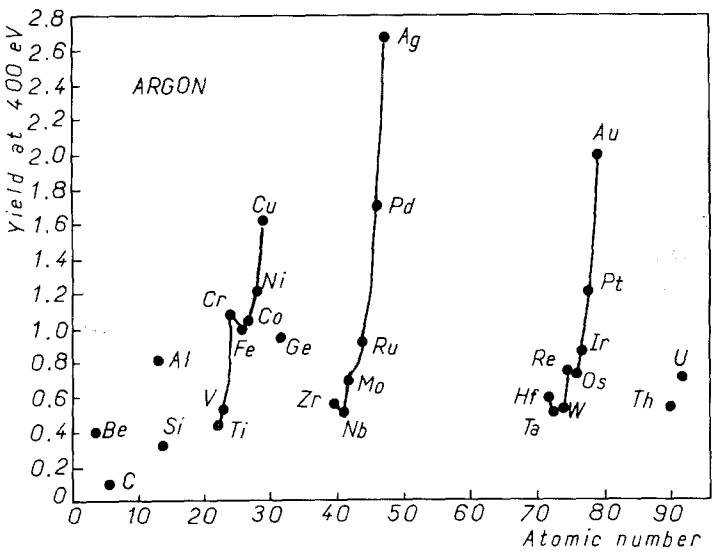

Figure 14 Summary of sputtering yields for a large number of 45 keV ions bombarding tantalum, copper and silver targets [13]. The observed evolutions include the effects of the mass of target atoms and ions, the binding energy of target atoms and chemical effects due to the nature of the bombarding species. Large ion doses were used in these experiments and compounds are formed by the target (Ta, Cu, Ag) and some implanted ions.

yield of each element varies as the surface binding energy $U'_{s,i}$ of the i element [20].

$$S'_i(E_1) = C_i\left(\frac{U_{s,i}}{U'_{s,i}}\right)^{1-2m} S_i(E_1) \qquad (17)$$

with $0 < m < 0{,}2$. The least bound species tend to sputter preferentially.

For not too different masses of elements i and j in a binary target i–j, the ratio of the partial sputtering yields may be approximated by the expression [20]:

$$\frac{S'_i}{S'_j} = \frac{C_i}{C_j}\left(\frac{M_j}{M_i}\right)^{2m}\left(\frac{U'_{s,j}}{U'_{s,i}}\right)^{1-2m}. \qquad (18)$$

For $U'_{s,j} \simeq U'_{s,i}$ the lighter species sputter preferentially.

The equations are more complicated in the case of very different masses, and all possible cases of preferential sputtering may be predicted from Jimenez equations developed by Sigmund [20] and Jimenez-Rodriguez *et al.* [30]. The evaluation of sputtering yields were tested for a few binary systems, and fit well with experimental results [30].

4.4. Limits of the model

We previously stated that the above equations are only valid in the case of a linear collision cascade. Now the Sigmund model neglects the influence of the target crystallinity, which determines the mean range $\langle x \rangle$ of ions and values of E_d and U_s. The variation in the channeling of the ion beam with the crystallographic orientation of the surface induces a simultaneous variation of the energy deposited in the outermost atomic layers of the surface. This phenomenon accounts for the observed changes in the sputtering yield of a crystal according to its surface orientation (Fig. 15). In a crystalline target, the requisite energy E_d to produce an effective displacement depends on the direction of the recoil, because of the possibility of a further substitution during a secondary collision or of a substitution between the recoiling atom and a vacancy. The value of E_d

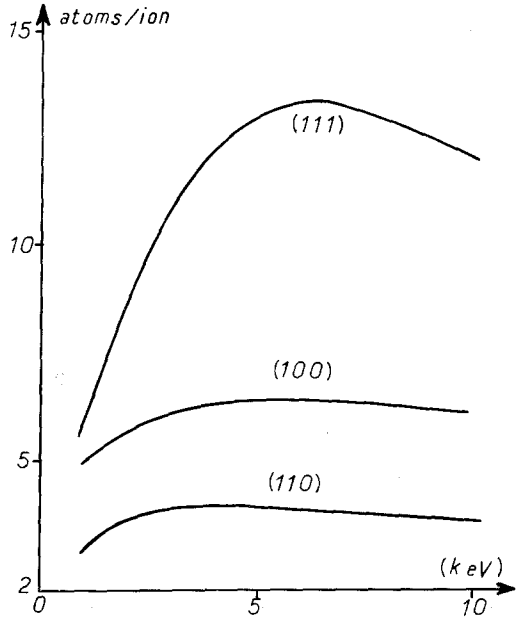

Figure 15 Variation of the sputtering yield of a silver target with its surface orientation and the energy of argon ions (after Magnuson and Carlson, 1963) [11].

is greatest for atoms recoiling along dense atomic rows. When considering the energy range of recoiling atoms, there is a minimal value $E_d(\min)$ for which a few atoms will be displaced if recoiling in an optimal direction, and there is a maximal value $E_d(\max)$ for which the probability of a displacement is equal to unity whatever the direction of the recoil. One must also consider focusons which may make a small contribution to sputtering. The surface potential does not have a simple value, but depends on the surface orientation. However, such variations in the range of ions, the displacement energy and the surface potential are averaged in a polycrystalline target; in this case, the measured sputtering yield may be considered as equivalent to that of an amorphous target.

The main limit of the Sigmund model (and other models based on the same concepts) with respect to computer simulations of sputtering events, is that cumulative changes in the surface composition due to successive cascades are put into equations with difficulty. In the case of monatomic targets, the sputtering yield varies progressively with the dose of implanted ions. The change of the target composition accounts for the deviation between the discontinuous variation of S with the mass of ions observed on Fig. 13 and the continuous variation predicted by the theory. Elements of a theory were proposed by Sigmund in recent papers [19, 21] to estimate the effect of heterogeneous redistribution of the elements in outermost layers of polyatomic targets with increasing ion fluences on their respective sputtering yields.

Note also that the sputtering yield may differ from the expected value at the beginning of the erosion process because of surface contamination. In particular, a metallic surface is generally covered with an oxide film when exposed to oxygen partial pressures exceeding 10^{-8} torr; this oxide is continuously replaced when the ion bombardment density is such that the sputtering rate of the surface is lower than the covering rate of the surface with adsorbed atoms (Fig. 16) [45, 46].

5. Radiation damage: changes in the structure of the surface due to sputtering

The number of atoms displaced during each collision cascade may be estimated by the semi-empirical Kinchin–Pease formula [12]

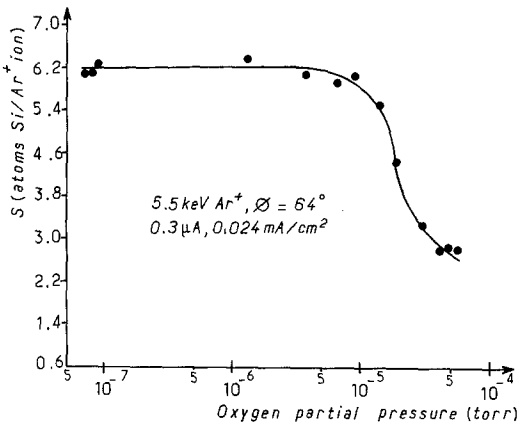

Figure 16 Variation of the sputtering yield of a silicon target with the oxygen partial pressure [45].

$$N_d(E_1) = \frac{E_1}{2E_d} \tag{19}$$

It was previously stated that the value of E_d is determined with difficulty. In most materials, experimental values of $E_d(\min)$ are in the range 10 to 50 eV; they are of the order of 40 to 50 eV in metals and lower in semiconductors [30]. Values of $E_d(\max)$ were estimated as $2.6E_d(\min)$, and the average value corresponding to a 50% probability of displacement is $2E_d(\min)$ [35–37]. Thus $N_d(E_1)$ may be estimated using experimental values of $E_d(\min)$:

$$N_d(E_1) = \frac{E_1}{4E_d(\min)} \tag{20}$$

A 1 keV argon ion displaces about 12 atoms in a nickel or copper target and 25 in silicon. The same ion sputters about 3 nickel or copper atoms, and 1 silicon atom (according to various calculations [7, 48]). In this first Section on radiation damage, the structure of outermost layers and the surface topography resulting from these displacements and sputtering events will be discussed.

5.1. Values and distribution of damages in the cascade volume

The displacement of atoms induces the formation of Frenkel pairs within the cascade volume. At the end of the collision cascade (10^{-13} sec) a large part of these vacancies and interstitials are eliminated during lattice vibrations, by mutual recombination of pairs which are close enough in the lattice or by annihilation at the target surface [11]. Residual defects are not uniformly distributed within the cascade volume, since primary

recoiling atoms are implanted at the periphery of this volume. A vacancy-rich zone is formed in the cascade core and interstitials segregate at its periphery [11]. This mechanism is confirmed by field-ion microscopy experiments [49]. In both zones the point defects may collapse into dislocation loops, which were observed by many authors by transmission electron microscopy [32, 50–61]. Interstitial loops are rather created under light ion irradiation, while heavier ions rather creates vacancy loops [32, 55]: vacancy clusters form when the deposited energy density exceeds the spike threshold. After a mild anneal, individual defects are eliminated at the target surface or form loops.

If metallic targets remain generally crystallized, semiconductors [62] and oxides [63] are often amorphized after a medium or high dose irradiation (10^{14} to 10^{17} ions cm^{-2}): for instance, the amorphization of silicon under a 5 keV argon bombardment is well known in SIMS.

5.2. Roughness induced by sputtering in a single-phase target

Sputtering induces roughness even on an amorphous target, since it is a random process. If only atoms located at the very surface could be sputtered during each collision cascade, a fraction of the first layer would be ejected by the first ion, then the second ion would sputter some remaining atoms of the first layer and uncovered atoms of the second one, and so on. This crude scheme accounts for a statistical widening of the surface rugosity [64] and summarizes the so called SLS model [65]. But one must take into account that atoms and clusters are sputtered from 2 or 3 layers during each cascade and that a part of the rugosity is smoothed by a surface diffusion of atoms, enhanced by radiation damage. The alteration of the resolution of interfaces in alternating layers of amorphous or microcrystalline materials was estimated by simulation using a Monte Carlo method [26]. In the case of gold and platinum layers 4 nm thick, bombarded by 2 keV argon ions, the resolution was constant over 20 successive layers, thus demonstrating that the surface topography was nearly constant after sputtering of a few nanometres and of the order of the ion range. However, peeling of the target surface one layer at a time is an unrealistic simplification.

In a crystalline target, differences in the channeling of ions, differences in the value of the binding energy U_s according to the surface orientation, and to a lesser extent the contribution of focusons, induce an etching of the grains. This effect is used to observe the structure of the material, especially in those difficult to etch by chemical or electrochemical means. Moreover in each grain, sputtering induces periodic structures (cones and surface waves of 100 to 1000 nm), which are due to various processes [58]:

(a) Dechanneling at dislocation lines, inherent to a coalescence of radiation damage,

(b) Local modifications of the surface binding energy, due to fluctuations in the surface orientation. Such variations induce also a differential sputtering in the vicinity of dislocations and grain boundaries.

This fine rugosity may be of importance in quantitative AES, since the analysed area changes [96] and because of the anisotropy in the emission and the adsorption of Auger electrons [97]. One must also take care of this effect when cleaning the surface of a monocrystal by sputtering, before a study of physical properties of the oriented surface or a study of its reactivity with gas. If the surface is annealed during or after sputtering, a possible influence of the irradiation on faceting, or on the distribution and density of dislocation networks, or on the formation of periodic structures and porosities, must be checked by electron microscopy. Fortunately such effects occur mostly in targets bombarded with high-energy ions.

On the other hand, the etching of grains is a crucial limitation to depth profiling by any technique linked with sputtering. Its inhibitory influence on the depth resolution of interfaces with AES was studied by Mathieu [98]. The author observed that the apparent thickness of interfaces, Δl, increases with the thickness of the material that needs to be removed before reaching the interface to be studied. This alteration of the interfaces resolution is mainly due to a cumulative relief, since other factors affecting the depth resolution (see Section 6) do not depend on the sputtered thickness. An empirical law was proposed, which relates Δl to the sputtered depth l, the energy of ions E_1 and the contribution of other factors a:

$$\Delta l = a + b(E_1 l)^{1/2} \qquad (21)$$

5.3. Roughness induced by differential sputtering from a multi-phase target

Another cause of cone formation is the differ-

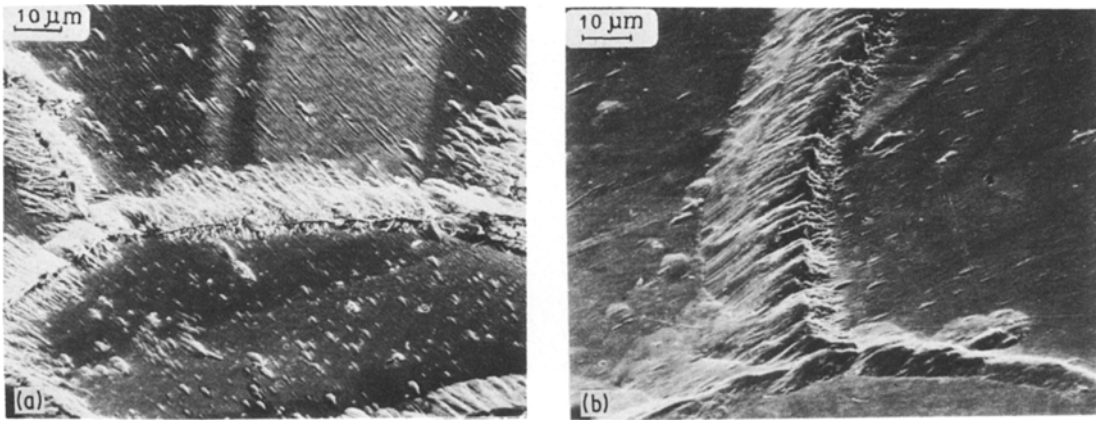

Figure 17 Formation of cones during sputtering by 5.5 keV argon ions in a Cu–Be 2% sample containing BeO precipitates (particularly along grain boundaries) [68].

ential sputtering of precipitates or segregated impurities, which have a smaller sputtering yield than the matrix [58, 66, 67]. These cones remain on the surface for a long time even after the inclusion has been sputtered, because the generators of the cone are parallel to the direction of incidence of ions. Fig. 17 shows such cones formed during a 5 keV argon bombardment in a Cu–2 at% Be target, containing BeO precipitates along grain boundaries and within grain [68]. The BeO precipitates have a smaller sputtering yield than the copper matrix. The figure illustrates the fact that the generators of cones formed along various grain boundaries are parallel to the same direction.

On the other hand, such differential sputtering induces a continuous change in the surface density of the inclusions, until a steady-state density n_s is obtained, different from the original one n_s^0. The thickness x of the matrix, which must be sputtered to get the steady-state, was calculated in the case of spherical inclusions of radius R [69]:

$$x = 2R\frac{S_{\text{matrix}}}{S_{\text{precipitates}}} \tag{22}$$

The steady-state density is:

$$n_s = n_s^0\frac{S_{\text{matrix}}}{S_{\text{precipitates}}} \tag{23}$$

Thus gradients in the distribution of precipitates will be quantified with difficulty.

6. Radiation damage: changes in the superficial and the depth compositions of the target

Ion implantation, displacements and sputtering of atoms during the collision cascade, and the diffusion of species at the end of the cascade, modify the composition of the surface, which is analysed by AES or ESCA. But they also change the distribution of atoms in the cascade volume. Depth profiles in heterogeneous targets are altered, particularly the resolution of interfaces between successive layers.

6.1. Implanted ions

Each implanted ion is sputtered during a following collision cascade, but at each instant a noticeable amount of the bombarding species remains in the target. A crude estimation of the steady-state content is:

$$C_i = p\frac{1}{S+1} \tag{24}$$

in which p is the implantation probability; it is about unity since few ions are backscattered. Estimated and measured values of C_i for most materials sputtered by a few keV argon ions are in the range 5 to 15% [12, 26, 70].

Inert species such as helium, argon, xenon which are insoluble in metals (solubility $< 10^{-10}$), may precipitate as bubbles, especially when sputtering is followed by a mild annealing of the target [58]. Irradiation-enhanced diffusion may also promote such a precipitation in particular targets. Reactive species tend to segregate on linear defects and at the surface, or to form a compound with the matrix elements. For instance oxide precipitates were observed in metals bombarded with high oxygen doses (NiO in nickel, Fe_3O_4 in iron) [71, 72] or $CuAl_2$ precipitates in aluminium bombarded with copper ions [58]. Elements such

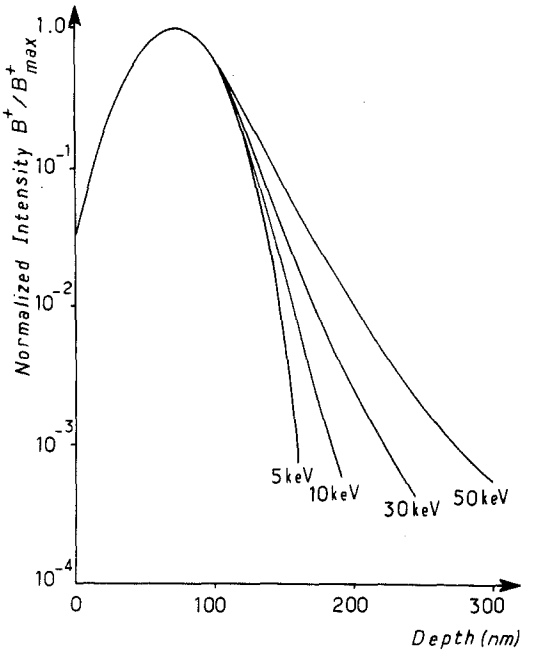

Figure 18 Depth profiles of boron in a silicon target implanted with 20 keV B^+ ions. Parameter is the energy of the primary Ar^+ ions used in the SIMS analysis [77, 78].

as phosphorus or boron implanted in nickel segregates at the surface [70], because of their enhanced diffusion during successive cascades.

6.2. Recoil implantations and cascade mixing

One must distinguish atoms displaced during primary recoils from those displaced during the cascade of secondary recoils. Their mean free path are different and their displacements have two different effects on the depth distribution of atoms in the target: for instance on the broadening of interfaces in a multilayer target. There exist many papers illustrating these two effects [74–78], and theories of these processes have been outlined by various authors [19, 73, 75, 79, 80].

6.2.1. Recoil implantations

During primary recoils atoms are pushed a long way to the target. Their implantation profile $f(x)$ was described in Section 3.2. These anisotropic displacements account for assymetric deformations of depth profiles over distances of the same order of magnitude as the range $\langle x \rangle$ of ions and recoiling atoms.

The effect is illustrated in Fig. 18, which shows the distortion of the distribution of implanted boron in a silicon target introduced during further analysis of this distribution by SIMS [78]. The higher the energy of argon ions used for the analysis, the larger is the deformation of the initial Gaussian boron distribution. The effect is particularly obvious in the chosen example, because the recoil implantation of atoms is selective. Boron and silicon atoms have very different masses and boron atoms are preferentially displaced during primary collisions.

Experiments performed by Seran [74] indicate that the lengthening of the profiles is nearly proportional to E_1/S.

6.2.2. Cascade mixing

During a cascade of secondary recoils, the displaced atoms migrate at random over short distances. This second effect of isotropic cascade mixing was put into equation by Andersen [75] and Carter [73]. Andersen considers atoms located in a plan parallel to the target surface at a depth x. Their initial of the Dirac-type distribution $\delta(x)$ is deformed into a Gaussian of full width Δ at half-maximum given by:

$$\Delta = 2Rn^{1/2}. \tag{22}$$

R is the mean free path of atoms with a low kinetic energy (near E_d) and n is the number of displacements of each atom before it is sputtered:

$$n = \frac{N_d(E_1)}{S} = \frac{E_1}{4E_{d\,min}} \times \frac{U_s}{0.042\alpha_N(M_1/M_2)\sigma_n(E_1)} \tag{23}$$

The widening Δ of the $\delta(x)$ function increases with the energy of incident ions E_1 and the ratio M_1/M_2. For 1 keV argon ions, Δ is of the order of 3 nm in silicium and 1 nm in copper or nickel [75].

Simulations already mentioned [26] of the sputtering of alternating layers of gold and platinum give comparable values of Δ, of the order of 2 nm (Fig. 19). In this case the alteration of the resolution is primarily due to cascade mixing since gold and platinum have nearly the same atomic mass, displacement energy and surface binding energy.

6.3. Enhanced diffusion

In some cases, the deformation of a profile is too substantial to be attributed only to recoil implantations and cascade mixing. Moreover, the tail

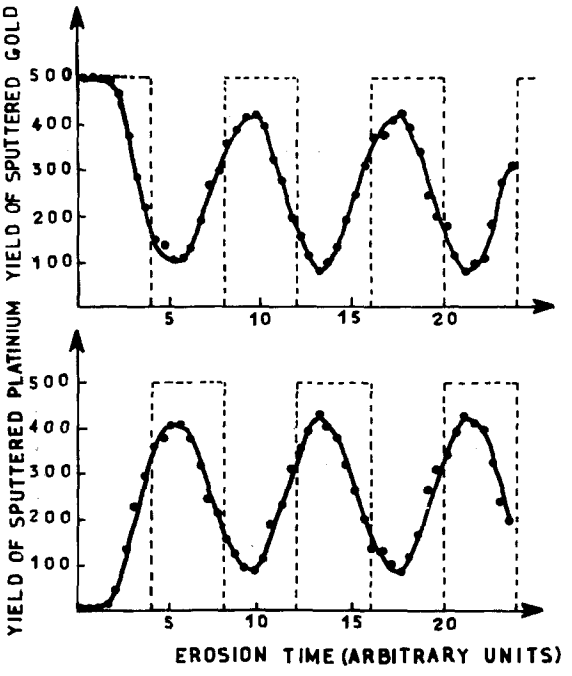

Figure 19 Simulation of the sputtering of alternating layers of gold and platinum 4 nm thick, under a 2 keV argon bombardment.

increases with the bombardment density, while the number of recoiling atoms depends only on the ion dose. Then the effect can be ascribed only to an enhanced diffusion of atoms induced by radiation defects [46, 66].

An example is the growth of oxide films formed on a nickel surface when exposed to an oxygen partial pressure (10^{-5} torr) under increasing densities of bombardment by argon ions (energy 6.6 keV) [46]. After a few minutes of exposure to oxygen and simultaneous sputtering of the surface, an equilibrium thickness of the film is obtained. The profiles were determined by SIMS under vacuum of 10^{-7} torr and using a constant density of bombardment by 5.5 keV argon ions to sputter the different films (see Fig. 20). The knock-on effect (recoil implantation) is the same for all profiles (formed without bombardment). We obtained the rather striking result that the thickness of the oxide film increased with the bombardment density, in spite of the increasing number of oxygen atoms removed of the surface by sputtering. The enhanced diffusion of oxygen was ascribed to an accumulation of defects (inter-

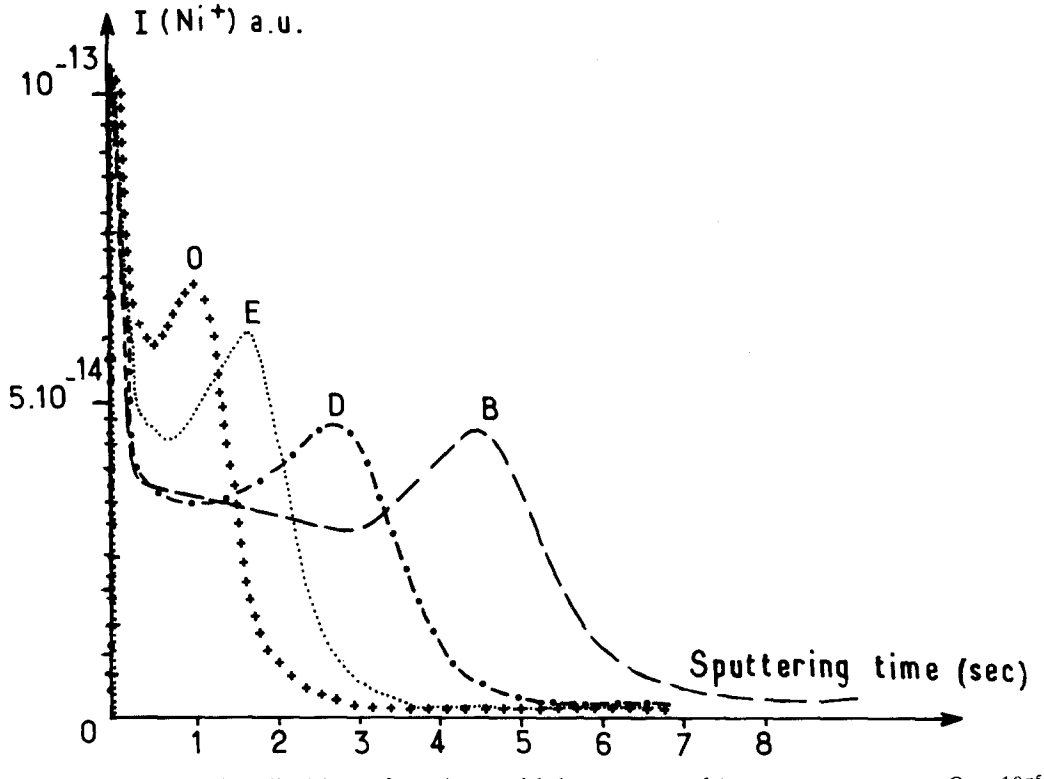

Figure 20 Depth profiles of oxidized layers formed on a nickel target exposed to an oxygen pressure $pO_2 = 10^{-5}$ torr and simultaneously sputtered by increasing densities of 5.5 keV argon ions. Curve (0) - without bombardment. Curve (E) - density of bombardment ip = 0.05 μA mm^{-2}. Curve (D) - ip = 0.1 μA mm^{-2}. Curve (B) - ip = 3 μA mm^{-2}. All profiles were obtained by SIMS with a constant density of bombardment by 5.5 keV ions: ip = 3 μA mm^{-2}.

stitials or vacancies), which could not be eliminated during the interval of time between 2 successive collision cascades in a same volume of the target, when this interval decreases.

In other cases, the diffusion may facilitate the segregation of the matrix constituents [93] or of the implanted species at the surface [70].

6.4. Change in the superficial composition due to selective displacements of atoms

In a binary system, the lighter species is preferentially sputtered. Kelly calculated that within the linear cascade regime, most of the effect is certainly due to selective displacements during primary collisions as for recoil implantation [39].

Numerous studies deal with this effect [81–92]. The first evidence of an altered composition of surfaces was obtained by Gillam [84], studying changes in the electronic diffraction patterns of Cu–Au and Pd–Ag alloys bombarded with He^+, Ar^+ or Xe^+ ions: an increase of a factor 2 was observed for the superficial concentration of gold on a Cu_3Au alloy sputtered by argon ions of 0.4 to 4 keV. Further examples were obtained using AES or Rutherford backscattering on Ag–Au, Cu–Au [81, 87, 91], Al–Cu [92], Pt–Si, Ni–Si, In–P, Ge–Si [81, 83] systems.

The modification of the surface composition is the greater, the more the masses of atoms A and B differ. It depends also on the energy of ions. An altered layer is progressively formed of which thickness t is approximately the range of ions [81–84, 89]: about 1 nm for 0.5 keV argon ions and 4 nm for 2 keV argon ions in most alloys. After an interval of time corresponding approximately to the sputtering of a thickness t [83, 89], a steady-state composition of the surface set up. Once this steady-state is obtained, further sputtering of the altered layer induces a composition change in a layer of the same thickness. Thus the composition of the sputtered volume, of which are extracted the particles analysed in SIMS is that of the bulk. But the surface analysed in AES is changed.

Since the composition of the sputtered volume is that of the bulk, the sputtering yields of both species S^A_{AB}, S^B_{AB} are proportional to the bulk concentration C^A_b, C^B_b during the steady-state:

$$S^A_{AB} = S_{AB} C^A_b, \qquad S^B_{AB} = S_{AB} C^B_b \tag{24}$$

in which S_{AB} is the global sputtering yield of the target.

On the other hand S^A_{AB} is the product of the superficial concentration C^A_s by the ejection probability p^A of each atom A:

$$S^A_{AB} = p^A C^A_s, \qquad S^B_{AB} = p^B C^B_s \tag{25}$$

From Equations 24 and 25 it can be deduced that:

$$\frac{S^A_{AB}}{S^B_{AB}} = \frac{C^A_b}{C^B_b} = \frac{P^A}{P^B}\frac{C^A_s}{C^B_s} \tag{26}$$

The modification of the surface composition is counterbalanced by the ratio of the ejection probabilities during the steady-state.

Several authors [28, 81, 84] proposed the hypothesis that p^A, p^B are independent of the concentrations and equal to those in pure matrix A and B. Then their ratio p^A/p^B would be the ratio of elemental yield S^A_A/S^B_B:

$$\frac{C^A_s}{C^B_s} = \frac{C^A_b}{C^B_b}\frac{S^B_B}{S^A_A} \tag{27}$$

But there is evidence that the global sputtering yield S_{AB} of alloys and those of each element S^A_{AB}, S^B_{AB} may be larger than either elemental yield S^A_A, S^B_B: for instance in Cu_3Au [89, 91]. In such cases p^A, p^B are certainly dependent of the concentrations. It was clearly shown in Section 4 that the ejection probability of atoms is not determined by atomic parameters only but also by the properties of the matrix, which in some cases are very different from those of pure A and B.

On the other hand, a question which is not resolved is the meaning of the determined concentrations C^A_s, C^B_s, since the composition of the altered layer is heterogeneous in depth (almost within the linear cascade regime). For example, Liau *et al.* [81, 82] determined quantitatively the gradient of composition induced by an argon bombardment in a Pt–Si target (Fig. 21). The energies of argon ions used in these experiments are greater than the energy range used in sputtering experiments, but the interest is that the altered layers are thick enough to be quantitatively analysed by Rutherford backscattering of high-energy ions (1.9 MeV $^4He^+$ ions). The reader should consult [1] for further details on this technique.

Fig. 21 shows that the thickness of the altered layer increases with the energy of sputtering ions, and is of the order of their penetration depth. In

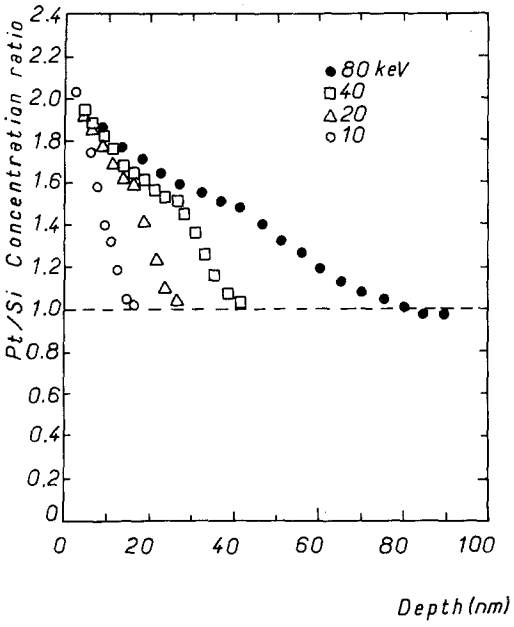

Figure 21 Steady-state Pt/Si concentration profiles in altered layers formed on Pt–Si samples sputtered by 10, 20, 40 and 80 keV argon ions. The profiles were obtained by the Rutherford backscattering technique using 1.9 MeV $^4He^+$ ions [81, 82].

this particular case, no change in the composition of the outermost layers is observed when the energy of argon ions varies between 10 and 80 keV: the ratio of the sputtering yields S^{Pt}/S^{Si} and remains constant. But the altered layers do not have a constant composition in depth.

The correction of preferential sputtering effects in quantitative analysis of sputtered surfaces by AES or XPS would need the knowledge of this depth distribution, in order to calculate the emission and absorption coefficients of electrons by each atomic layer. Theories have been outlined to calculate the change in the depth composition within the linear cascade [79, 80] or spike [42] regimes, but the only usable procedure for the correction of AES or XPS data is the comparison of the measured signals with those of standards sputtered in the same conditions.

6.5. Change in the superficial composition due to a difference in the binding energy of atoms, U_s

The most volatile species is preferentially sputtered: for example, magnesium in alloys or oxygen in oxides [39]. Fig. 22 shows, for example,

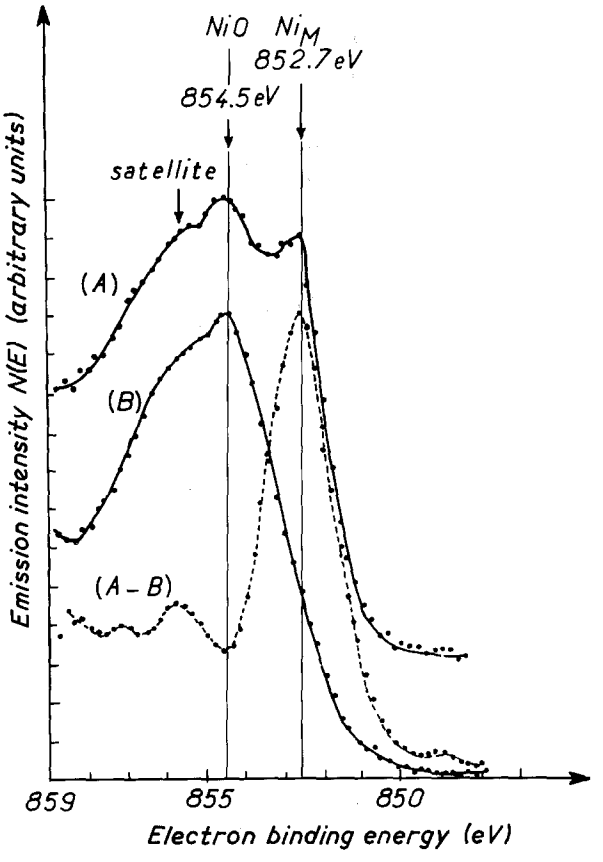

Figure 22 X Photoelectron Spectra recorded on a NiO film 2 μm thick, formed at 600° C on pure nickel. Curve (A) - after sputtering about 10 nm with 1 keV argon ions. Curve (B) - after an exposure of 100L to oxygen. Curve (A-B) - difference of the preceeding N(E) curves, putting into evidence the nickel metal peak.

the modifications of the Ni2*p* band observed on the XPS spectrum of a thick NiO film after a few minutes sputtering with 1 keV argon ions [99]. The peak at 852.7 eV corresponds to the binding energy of 2*p*3/2 electrons in the metal, suggesting the presence of an appreciable proportion of Ni–Ni bonds at the surface. This peak disappears after an exposure of 100 L (1 Langmuir = 10^{-6} torr) to oxygen.

In the case of insulating oxides the preponderant sputtering process might be a thermal spike rather than a collision cascade. Kelly [39] made an attempt to differentiate oxides in terms of their thermodynamic stability. Considering their respective free energy of dissociation ΔF_T^0 (i.e. their oxygen vapour pressure) in a range of temperature $T = 3500$ to 4500 K, Kelly confirmed that:

(a) Some oxides such as Fe_3O_4, Fe_2O_3, MoO_2, CuO, CdO, are unstable at temperatures above 3500 K, and their surface is depleted in oxygen when bombarded by noble gas ions.

(b) Other oxides, such as Cr_2O_3, FeO, ZnO, MnO, are stable and their surface is not depleted in oxygen.

Exceptions are oxides such as NiO, PbO, TiO_2 which are unstable and show a bombardment-induced loss of oxygen when sputtered by some ions, but not for other bombarding species.

The choice of an apparent temperature in the range 3500 to 4500 K was made on the basis of a thermal spike model [15], but this process of dissipation of the incident energy must be considered as a radiolysis effect, similar to that observed under an electronic bombardment in AES [94, 95], rather than as a sputtering process. Radiolysis effects in titanium oxides under ionic and electronic bombardment were extensively studied by Mathieu *et al.* [94]. No satisfactory quantitative estimates of these effects can be made at present.

7. Conclusion

The theories of Lindhard and Sigmund do not take into account the structure of materials. However, they provide an interpretation for most of the observed phenomena: the influence of the atomic number, mass of ions and target atoms, the binding energy of atoms to the surface and the energy of ions on the sputtering yield and on alterations of the surface composition.

The peeling of the surface of a crystal one layer at a time is an unrealistic model, because of the microscopic rugosity induced by the bombardment, the cascade mixing of atomic layers, the recoil implantations and the diffusion of residual defects. However, these effects are minimized when using ions of low energy for sputtering. Nevertheless, these defects and the implantation of ions in the target must be considered in fundamental studies of surface physical properties.

Many authors have focused their attention on the errors in the experimentally determined composition profiles resulting from the form of the sputtering relief, because this is a limiting factor in applied studies of thin films. We must emphasize the fact that the distortions of most published profiles are due to experimental artefacts or to structural features of the films rather than to any intrinsic limits of the physical process used to determine the profile. The resolution is often affected by a Gaussian shape of the crater or by a misalignment of the ion beam [100]. The most elegant method for improving the depth resolution of profiles is not one based on correcting the profiles in terms of a mathematical function describing the crater shape [100], but rather one based on optimizing the optics of the ion gun (appropriate scanning of the ion beam) or the exact method of collection of the particles to be analysed (additional lenses and diaphragms). Nevertheless, the morphology of films must be taken into account. For instance, polycrystalline films formed at high temperature on a surface (by vapour deposition, reaction with a gas or ion-coating, etc.) show microscopic heterogeneities of thickness corresponding to their grain size: these heterogeneities determine the apparent width of the interface between the film and the substrate deduced from sputtering profiles [101]. Porosity or cracks also affect the depth resolution since the atomic density of the film is locally changed. The rugosity due to the differential sputtering of grains may be diminished by using grazing ion bombardment or by sputtering the surface with heavy ions.

However, the most limiting factor for electron spectrometry on sputtered surfaces is certainly the modification of their composition (and hence electronic structure) by the sputtering process. The extent of this modification cannot as yet be predicted quantitatively; it can only be checked by comparisons using homogeneous standards

sputtered with increasing doses of various types of ions, accelerated to a range of energies.

Acknowledgements

The author is grateful to H. Bernas and J. Chaumont for valuable discussions and providing certain papers, to Professor R. W. Cahn who improved the clarity of the manuscript, and to Mme B. Jory for turning my draft into a clear final product.

References

1. "Material Characterization using Ion Beams", published in NATO Advanced Study Institute Series 28, edited by J. P. Thomas and A. Cachard (Plenum Press, London and New York, 1978).
2. P. SIGMUND, "Inelastic Ion-Surface Collisions", edited by N. H. Tolk (Academic Press Inc., New York, 1977) p. 121.
3. J. LINDHARD, M. SCHARFF and M. E. SCHIOTT, *Kgl. Danska Videnskab. Selskab. Mat. Phys. Medd.* **33** (1963).
4. J. LINDHARD, V. NIELSEN and M. SCHARFF, *ibid.* **36** (1968).
5. J. B. SANDERS, Thesis, University of Leiden (1968).
6. *Idem, Can, J. Phys.* **46** (1968) 455.
7. P. SIGMUND, *Phys. Rev.* **184** (1969) 383.
8. *Idem. Rev. Roum. Phys.* **17** (1972) 823.
9. *Idem*, "Sputtering yield of ion bombarded Solids", Third National Conference on Atomic Collision in Solids, Kiev, USSR, October 1974.
10. *Idem*, in "Radiation Damage Processes in Materials", published in NATO Advanced Study Institute Series, edited by C. H. S. Dupuy (Noordhoff International Publishing, Leyden, Netherland, 1974).
11. CHR. LEHMANN, "Interaction of Radiations with Solids and Elementary Defects Production", edited by S. Amelinckx, R. Gevers and J. Nihoul, Series of books "Defects in Crystalline Solids", **10**, (North Holland Publishing Company, Amsterdam, 1975).
12. G. CARTER and J. S. COLLIGON, "Ion Bombardment of Solids" (Elsevier Publishing Company Inc., New York, 1968).
13. D. E. ALMEN and G. BRUCE, *Nucl. Instrum. Methods* **11** (1961) 279.
14. W. JÄGER, *J. Microsc. Spectrosc. Electron.* **6** (1981) 437.
15. R. KELLY, "Collisional, thermal and electronic sputtering", in Proceedings of the International Conference on Ion Beam Modification of Materials, Budapest (1978), published in the journal *Nucl. Instrum. Methods.*
16. B. J. GARRISON, N. WINOGRAD and D. E. HARRISON, *J. Chem. Phys.* (1978).
17. D. E. HARRISON, B. J. GARRISON and N. WINOGRAD, in Proceedings of the Second International Conference on S.I.M.S., Stanford, California (1979), book published in "Springer Series in Chemical Physics" **9**, (Springer Verlag, Berlin, Heidelberg, New York, 1979) p. 12.
18. K. KANAYA, K. HOSOU, K. KOGA and K. TOKI, *Jpn. J. Appl. Phys.* **12** (1973) 1297.
19. P. SIGMUND, A. OLIVA and G. FALCONE, in Proceedings of the Ninth International Conference on Atomic Collisions in Solids, Lyon, France (1981), published in the journal *Nucl. Instrum. Methods* (1982).
20. P. SIGMUND, in "Sputtering by Particle Bombardment", edited by R. Behrisch, Series of books "Topics in Applied Physics" **47**, (Springer Verlag, Berlin, Heidelberg, New York, 1981) p. 9.
21. N. ANDERSEN and P. SIGMUND, *Mat. Fys. Medd. Dann. Vid. Selsk.* **39**, (1974).
22. D. E. HARRISON and C. B. DELAPLAIN, *J. Appl. Phys.* **47** (1976) 2252.
23. M. T. ROBINSON and I. M. TORRENS, *Phys. Rev.* **9** (1974) 5008.
24. T. ISHITANI, K. MURATA and R. SHIMIZU, *Jpn. J. Appl. Phys.* **10** (1971) 1464.
25. S. T. KANG, R. SHIMIZU and T. OKUTANI *ibid.* **18** (1979) 1717.
26. M. L. ROUSH and T. D. ANDREADIS, *Rad. Eff.* **55** (1981) 119.
27. W. L. PATTERSON and G. A. SHIRN, *J. Vac. Sci. Technol.* **4** (1967) 343.
28. N. J. CHOU and M. W. SHAFER, *Surf. Sci.* **92** (1980) 601.
29. H. F. WINTERS and J. W. COBURN, *Appl. Phys. Lett.* **28** (1976) 176.
30. J. J. JIMENEZ-RODRIGUEZ, M. RODRIGUEZ-VIDAL and J. A. VALLES-ABARCA, *Rad. Eff.* **41** (1979) 165.
31. H. L. BAY, H. H. ANDERSEN, W. O. HOFER and O. NIELSEN, *Nucl. Instrum. Methods* **132** (1976) 301.
32. M. O. RUAULT, H. BERNAS and J. CHAUMONT, *Phil. Mag. A.* **39** (1979) 757.
33. M. W. THOMPSON, "Defects and Radiation Damages in Metals" (Cambridge University Press, 1969) p. 196.
34. M. SZYMONSKI and A. E. de VRIES, *Phys. Lett.* **63A** (1977) 359.
35. M. SZYMONSKI, H. OVEREIJNDER, A. HARING and A. E. de VRIES, *Rad. Eff.* **36** (1978) 189.
36. *Idem, ibid.* **37** (1978) 205.
37. H. H. ANDERSEN and H. L. BAY, *J. Appl. Phys.* **45** (1974) 953.
38. R. KELLY, *Rad. Eff.* **32** (1977) 91.
39. *Idem, Nucl. Instrum. Methods* **149** (1978) 553.
40. R. J. COLTON, J. S. MURDAY, J. R. WYATT and J. J. DE CORPO, in Proceedings of the 26th Annual Conference on Mass Spectrometry and Allied Topics (American Society for Mass Spectrometry, 1978).
41. A. BENNINGHOVEN and W. K. SICHTERMANN, *Anal. Chem.* **50** (1978) 1180.
42. P. K. HAFF, *Appl. Phys. Lett.* **31** (1977) 259.
43. H. H. ANDERSEN and H. L. BAY, *Rad. Eff.* **13** (1972) 67.
Idem, ibid. **19** (1973) 139.
44. D. ROSENBERG and G. K. WEHNER, *J. Appl. Phys.* **33** (1962) 1842.

45. A. E. MORGAN, H. A. M. de GREFTE, H. J. TOLLE, N. WARMOLTZ and H. W. WERNER, *Appl. Surf. Sci.* 7 (1981) 372.
46. J. C. PIVIN, C. ROQUES-CARMES and G. SLODZIAN, *Int. J. Mass. Spectrom. Ion Phys.* **31** (1979) 293.
47. H. H. ANDERSEN, "The Depth Resolution of Sputter Profiling", in Proceedings of the 3rd International Conference on Solid Surfaces, Vienna, 1977 (International Union for Vacuum Science, Technique and Application) (see also *Appl. Phys.* **18** (1979) 131).
48. K. KANAYA, *Jpn. J. Appl. Phys.* **12** (1973) 1297.
49. D. N. SIEDMAN, *J. Phys. F* **3** (1973) 393.
50. M. WILKENS, In "Application of Ion Beams to Metals", edited by S. T. Picraux (Plenum Press, New York, 1975) p. 441.
51. K. L. MERKLE, "Radiation Damages in Metals", edited by N. L. Peterson, (American Society of Metals, Metals Park Ohio, 1976) p. 58.
52. M. L. JENKIS, K. H. KATERBAU and H. WILKENS, *Phil. Mag.* **34** (1976) 1141.
53. L. E. THOMAS, T. SCHOBER and R. W. BALLUFFI, *Rad. Eff.* **1** (1979) 157.
54. D. I. R. NORRIS, *Phil. Mag.* **19** (1969) 527.
55. M. O. RUAULT, in "Application of Ion Beams to Metals", edited by S. T. Picraux, (Plenum Press, New York, 1973) p. 459.
56. *Idem, Phys. Rev. Lett.* **36** (1976) 1148.
57. *Idem,* Thèse d'Etat, Université Paris-Sud, Orsay, France (1975).
58. R. S. NELSON and D. J. MAZEY, *Rad. Eff.* **18** (1973) 127.
59. A. BOURRET and D. DAUTREPPE, *Phys. Status Solidi* **29** (1968) 283.
60. F. HAÜSSERMANN, *Phil. Mag.* **25** (1972) 537.
61. E. JOHNSON and J. A. YTTERHUS, *ibid.* **28** (1973) 489.
62. E. C. BARANOVA, *Rad. Eff.* **18** (1973) 21.
63. H. M. NAGUIB and R. KELLY, *ibid.* **25** (1975) 1.
64. A. BENNINGHOVEN, *Z. Phys.* **230** (1970) 403.
65. S. HOFMANN, *Mikrochim. Acta Suppl.* 7 (1977) 109.
Idem, Appl. Phys. **9** (1976) 59.
66. R. S. GVOSDOVER, V. M. EFREMENKOVA, L. B. SHELYAKIN and V. E. YURASOVA, *Rad. Eff.* **27** (1976) 237.
67. G. W. LEWIS, G. CARTER, M. J. NOBES and S. A. CRUZ, *Rad. Eff. Lett.* **58** (1981) 119.
68. O. LYON, Thèse de 3ème Cycle, Université Paris-Sud, Orsay, France (1974). M. C. MONTLOUIS, Thèse de 3ème Cycle, Université Paris-Sud, Orsay, France (1979).
69. G. BLAISE, O. LYON and C. ROQUES-CARMES, *Surf. Sci* **71** (1978) 630.
70. C. COHEN, A. V. DRIGO, H. BERNAS, J. CHAUMONT, K. KROLAS and L. THOME, *Phys. Rev. Lett.* **48** (1982) 1193.
71. M. M. TOCHIC, A. V. DRIGO, C. COHEN, L. THOME, J. CHAUMONT and H. BERNAS in Proceedings of the International Conference on Ion Beam Modification of Materials, 1980, published in the journal *Nucl. Instrum. Methods* **182–183** (1981) 303.
72. E. GIANI, D. K. MURTI and R. KELLY, in Proceedings of the Symposium on "Thin Film Phenomena. Interfaces and Interactions", published in *J. Electrochem. Soc.* **78** (1978) 443.
73. G. CARTER, D. G. ARMOUR, D. C. INGRAM, R. WEBB and R. NEWCOMBE, *Rad. Eff. Lett.* **43** (1979) 233.
74. J. L. SERAN, Thèse d'Etat, Université Paris-Sud, Orsay, France (1978).
75. H. H. ANDERSEN, "The Depth Resolution of Sputter Profiling", in 3rd International Conference on Solid Surfaces, Vienna, September 1977.
76. R. GROTZCHEL *et al. Rad. Eff.* **27** (1976) 237.
77. J. W. COBURN, *J. Vac. Sci. Technol.* **13** (1976) 1037.
78. F. SCHULTZ, K. WITTMAACK and J. MAUL, *Rad. Eff.* **18** (1973) 211.
79. P. SIGMUND, *J. Appl. Phys.* **50** (1979) 7261.
80. M. R. WILLIAMS, *Rad. Eff.* **59** (1981) 47.
81. Z. L. LIAU, W. L. BROWN, R. HOMER and J. M. POATE, *Appl. Phys. Lett.* **30** (1977) 626.
82. Z. L. LIAU, J. W. MAYER, W. L. BROWN and J. M. POATE, *J. Appl. Phys.* **49** (1978) 5295.
83. P. S. HO, J. E. LEWIS, H. S. WILDMAN and J. K. HOWARD, *Surf. Sci.* **57** (1976) 383.
84. E. GILLAM, *J. Phys. Chem. Solids* **11** (1959) 55.
85. M. L. TARNG and G. K. WEHNER, *J. Appl. Phys.* **42** (1971) 2449.
86. H. SHIMIZU, M. ONO and N. NAKAYAMA, *Surf. Sci.* **36** (1973) 817.
87. W. FÄRBER, G. BETZ and P. BRAUN, *Nucl. Instrum. Methods* **132** (1976) 351.
88. G. S. ANDERSON, *J. Appl. Phys.* **40** (1969) 2884.
89. H. F. WINTERS and J. W. COBURN, *Appl. Phys. Lett.* **28** (1976) 176.
90. D. T. QUINTO, V. S. SUNDARAM and W. D. ROBERTSON, *Surf. Sci.* **28** (1971) 504.
91. W. T. OGAR, N. T. OLSON and H. P. SMITH, *J. Appl. Phys.* **40** (1969) 4997.
92. W. K. CHU, J. K. HOWARD and R. F. LEVER, *ibid.* **47** (1976) 4500.
93. J. E. HOBBS and A. D. MARWICK, *Rad. Eff. Lett.* **58** (1981) 83.
94. H. J. MATHIEU, *J. Vac. Sci. Technol.* **14** (1977) 1023.
95. Y. AL. JAMMAL, D. POONEY and P. D. TOWNSEND, *J. Phys.* **C6** (1973) 247.
96. P. H. HOLLOWAY, *J. Elect. Spectrosc.* **7** (1975) 215.
97. D. ABERDAM, in "Journées d'Etude sur la Spectrométrie Auger", (1979), published as a special number of the journal *"Le Vide, les Couches Minces"*, (Société Française du Vide, Paris, 1979), 73.
98. H. J. MATHIEU, D. E. McCLURE and D. LANDOLT, *Thin Solid Films* **38** (1976) 281.
99. J. C. PIVIN and G. DUFOUR, unpublished work (1982).
100. J. B. MALHERBE, J. M. SANZ and S. HOFMANN, *Surf. Interface Anal.* **3** (1981) 235.

101. D. LOISON, J. C. PIVIN, J. CHAUMONT and C. ROQUES-CARMES, in Proceedings of the Conference on Ion Modification of Materials, Grenoble, France, 1982, to be published in the journal *Nucl. Instrum. Methods* (1983).

Received 1 September
and accepted 20 September 1982